Chemical Physics Impact 8 (2024) 100538

Contents lists available at ScienceDirect

Chemical Physics Impact

journal homepage: www.sciencedirect.com/journal/chemical-physics-impact

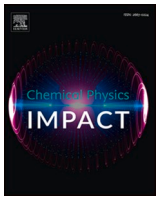

Full Length Article

A detailed theoretical investigation on intramolecular charge transfer mechanism of primary, secondary, and tertiary *p*-amino substituted benzaldehyde

Palash Jyoti Boruah [a], Venkatesh N [a], Anuva Samanta [b,*], Amit Kumar Paul [a,*]

[a] Department of Chemistry, National Institute of Technology Meghalaya, Bijni Complex, Laitumkhrah, Shillong, Meghalaya 793003, India
[b] Department of Chemistry, Victoria Institution (College), 78-B, A. P. C. Road, Kolkata, West Bengal 700009, India

ARTICLE INFO

Keywords:
TICT
DFT
Excited state dynamics

ABSTRACT

This article reports a detailed theoretical investigation on dual fluorescence properties of p-amino substituted benzaldehyde molecules by taking specifically *p*-N,N-dimethylaminobenzaldehyde (3° PABA), *p*-N-methylaminobenzaldehyde (2° PABA), and *p*-aminobenzaldehyde (1° PABA) molecules. The calculations are performed in gas phase as well as in butanol (BuOH) and dichloromethane (DCM) solvents. Twisted intramolecular charge transfer emission property is particularly looked at by scanning the potential energy curves as a function of -NR_2 (R = H/CH_3) rotation (twisting) angle. The results suggest that there are dual emission possibilities for 3° and 2° PABA molecules. Experimental validation is available for the former but not for the latter. 1° PABA, on the other hand, does not show any possibility of dual fluorescence except in BuOH. The theoretical absorption and emission spectra are also calculated and compared with experiment where it is available, and they are in close correlation. Excited state molecular dynamics simulations show that for 3° PABA, the molecule reaches to the 90° twisting angle and stays there with a probability higher than the same probability for 2° PABA. 1° PABA, on the other hand, had showed variations in the twisting angle from 0° to above 100°, but no evidence of this molecule to have considerable lifetime at 90° twisting angle.

1. Introduction

Organic molecules with donor-acceptor substituents showing dual emission properties has gained enough interest in the literature due to their wide applications [1–12]. Intramolecular charge transfer phenomenon is one of the most interesting sub-topics of dual emission properties [3–9]. Various para-amine substituted benzonitrile, benzaldehyde, benzoate derivatives, etc., are well explored for their useful applications in electro-optical switches, chemical sensors, fluorescence probes, etc [9–11]. A widely accepted model of the dual fluorescence of these molecules was proposed by Grabowski et al. [13,14]. and known as Twisted intramolecular charge transfer (TICT) and is depicted in Fig. 1 [8]. Other models of dual fluorescence, such as Wagging intramolecular charge transfer [15], planarized intramolecular charge transfer [16,17] were also proposed. 4-(N,N-dimethylamino) benzonitrile (DMABN) [1,2,7,13,14], *p*-N,N-dimethylaminobenzaldehyde (3° PABA) were studied experimentally as well as theoretically to understand their dual fluorescence based on TICT model [8]. It was shown that the fluorescence emissions are in plane and perpendicular orientations of –NMe_2 group with respect to the benzene ring plane as depicted in Fig. 1. 3° PABA exhibits a local emission (LE) at 370–390 nm, and a charge transfer (CT) emission at 490–510 nm in solvents with different polarity, according to Kawski et al. [18]. However, the CT emission of 3° PABA was detected at 600 nm, especially in DMF and ACN solvents, as reported by Kawski et al. [18]. and Grabowski et al. [19]. It was showed that complexing with cyclodextrin (CD) increases TICT emission of 3° PABA [20,21]. Research has reportedly been done on the impacts of gold nanoparticles on the intramolecular charge transfer (ICT) state of 3° PABA [22] as well as the interfacial electron transfer effects on it in TiO_2 and CdS semiconductor colloids [23]. As reported by Samanta et al. [8], when excited at 340 nm in polar liquids, DMABA emits two fluorescence. In addition to the local fluorescence at 385 nm, it also shows a long wavelength fluorescence band at about 520 nm, which is still weaker and is identified as generated from the ICT state. They have also explored the phenomena through computational DFT calculations. In addition, many other molecules are considered in the

* Corresponding authors.
E-mail addresses: anuva.samanta25@gmail.com (A. Samanta), amit.paul@nitm.ac.in (A.K. Paul).

https://doi.org/10.1016/j.chphi.2024.100538
Received 11 January 2024; Received in revised form 14 February 2024; Accepted 14 February 2024
Available online 15 February 2024

literature with the same perspective, for example, spirothiolactamized benzothiazole substituted N,N-diethylrhodol [24], excited state proton transfer of thiol [25], Nonadiabatic Relaxation Dynamics of 4-(N, N-Dimethylamino)benzonitrile (DMABN) [26], Time-resolved photoelectron spectroscopy of 4-(dimethylamino)benzethyne [27], photoprotection mechanisms of chalcones [28], substituent effects on excited-state intramolecular proton transfer and photophysical properties of fluorophores containing 4-diethylaminosalicylaldehyde [29], solvent-regulated enhancing fluorescence of benzimidazole derivative [30], development of smart-switch materials responsive to stimuli [31], etc. Despite the extensive studies as mentioned above of DMABN and 3° PABA, and other related molecular systems, the effect of primary, secondary, and tertiary amine on the dual emission property is not well explored.

In this work, the dual emission property of *p*-N,N-dimethylaminobenzaldehyde (3° PABA) molecule is examined in comparison with the primary and secondary amine analogues, namely, *p*-N-methylaminobenzaldehyde (2° PABA), and *p*-aminobenzaldehyde (1° PABA), in different solvents through theoretical calculations. The experimental data of 3° PABA is taken from the ref. 8 for reference. Two different solvents with different polarities are used, namely, butanol (BuOH) with polarity index (ε) 17.33 and dichloromethane (DCM) with the ε value of 8.93. The potential energy curve of the ground S_0 and excited S_1 states is scanned to understand the dual emission behavior and the emission wavelengths are computed. Finally, the non-adiabatic dynamics is performed to explore the possibility/probability of the ES-ICT phenomenon across the studied molecules. The article is organized as follows: Section 2 discusses the computational methodologies adopted for this work. Section 3 presents the results and the related discussion, where the potential energy curves, emission spectra, and the results from the dynamics are produced. Finally, the article is summarized in Section 4.

2. Computational methodology

The geometry optimization of all the substituted compounds of PABA were done with Density Functional Theory (DFT) with Becke, 3-parameter, Lee–Yang–Parr (B3LYP) functional [32,33] and 6–31G(d) basis set [34–36] in gas phase as well as in solvent phase using conductor-like polarizable continuum (CPCM) [37] and universal solvation (SMD) [38] models. This level of theory has been implemented in the past for DMABA, and the calculations were validated by experimental findings [8]. Therefore, DFT(B3LYP)/6–31G(d) level is accurate enough to draw conclusive statements. Time dependent DFT (TDDFT) calculations were performed in gas phase as well as in solvent phase to perform the geometry optimization at excited S_1 state, as well as to obtain both absorption and emission spectra. All these calculations are performed in Gaussian09 software [39].

To understand and validate the TICT phenomenon in the 3°, 2°, and 1° PABA, excited state on-the-fly dynamics was performed on the S_1 state of these compounds using NEWTON-X [40] program interfaced with COLUMBUS software [41]. For each molecule, 50 trajectories were integrated using the Wigner distribution model, which uses the normal modes of optimized ground state geometry. The trajectories were integrated for 300 fs with 0.5 fs integration time step. The integrations of the equations of motion were calculated through the Velocity-Verlet algorithm. Fifty (50) trajectories were generated at an excitation energy window of 5.54 ± 0.5 eV (5.54 eV = 223.8 nm; 5.04 eV = 246.0 nm, 6.04 eV = 205.3 nm) for 3° PABA, 4.65 ± 0.5 eV (4.65 eV = 266.6 nm, 4.15 eV = 298.8 nm, 5.15 eV = 240.7 nm) for 2° PABA, and 4.69 ± 0.5 eV (4.69 eV = 264.4 nm, 4.19 eV = 295.9 nm, 5.19 eV = 238.9 nm) for 1° PABA. The Absorption cross-section spectrum of 3°, 2°, and 1° PABA are shown in Fig. S1 of the Supplementary Material (SM). The dynamics were performed with CASSCF(6,6)/6–31G(d) method [42,43]. The orbitals for the Complete Active Space (CAS) consisted of π, π* orbitals and nonbonding orbitals. The orbitals are represented in Figs. S2–S4 of the SM. To include π orbitals of the benzene ring for the CAS calculation, an interchange was done in between HOMO-5 and HOMO-2 orbitals. The previous HOMO-2 (which is currently made HOMO-5) orbital of 3° PABA is shown in Fig. S5 of SM.

3. Results and discussion

3.1. Geometries and structural parameters

First, the minimum energy geometries of 1°, 2°, and 3° PABA are calculated for both S_0 and S_1 states. Fig. 2 displays the optimized geometries of these molecules S_0 state. As one can see that **–NR_2** (R = H/Me) group is coplanar (for tertiary amine) or nearly coplanar (for secondary and primary amine) with the benzene ring. Fig. S6 presents the same geometries at S_1 state. Table 1 reports the comparison of some crucial geometrical parameters of the S_0 and S_1 geometries of 3° PABA. Similar tables for 2° and 1° PABA are given in Tables S1 and S2. The geometrical parameters at S_1 state are very similar to the ones for S_0 state. These geometries are at the Franck Condon (FC) region. Thus, these geometries are associated with the absorption and local emission spectra.

It is believed that the CPCM model yields satisfactory results for charged transfer species. Hence, this model is focused to discuss the geometrical parameters as follows. The data presented in Table 1 indicates that the C3-N14 bond length for the CPCM model increases from 1.368 to 1.386 Å in the BuOH solvent and from 1.369 to 1.386 Å in the DCM solvent when excited from the S_0 to S_1 state. Conversely, the length of the C6-C11 bond decreases from 1.458 to 1.396 in both the BuOH and DCM solvents. However, upon examining the total distance between

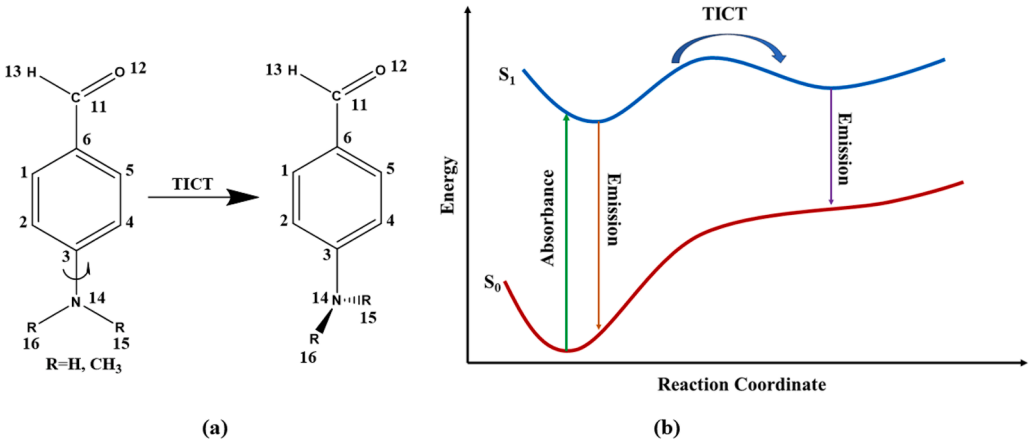

Fig. 1. Proposed TICT model (a) and the corresponding potential energy scan presented schematically.

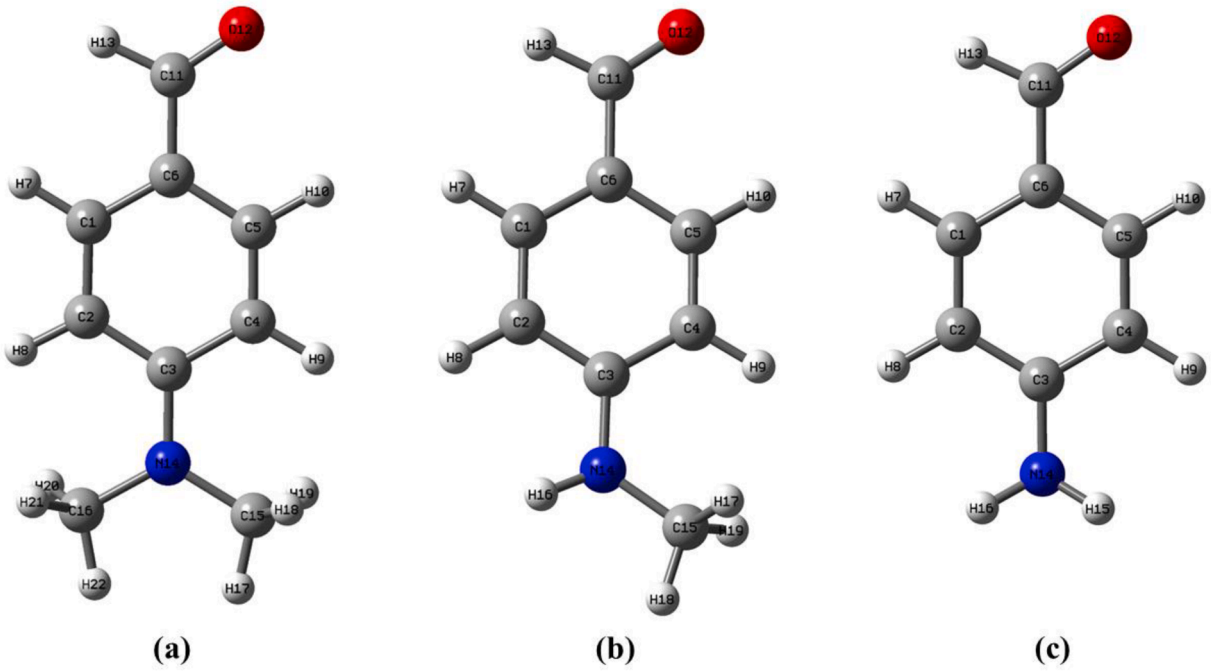

Fig. 2. Minimum energy geometry of (a) 3° PABA (b) 2° PABA (c) 1° PABA with B3LYP/6–31 g(d) level of theory for the gas phase calculation at S_0 state.

Table 1
Comparison of some crucial geometrical parameters of 3° PABA at S_0 and S_1 states with different solvent mediums.

Medium/ Solvent	State	Bond length C3-N14	Bond length C6-C11	Bond length C11-N14	Dihedral angle (C4-C3-N14-C15)	Dihedral angle (C5-C6-C11-O12)
Gas	S_0	1.377	1.467	5.684	-0.062	-0.002
	S_1	1.391	1.390	5.656	11.418	0.196
BuOH	S_0	1.366	1.452	5.664	-0.046	-0.004
(SMD)	S_1	1.388	1.398	5.661	-13.773	0.074
DCM	S_0	1.368	1.459	5.673	-0.044	-0.003
(SMD)	S_1	1.386	1.396	5.659	-11.326	-0.194
BuOH	S_0	1.368	1.458	5.672	-0.044	-0.002
(CPCM)	S_1	1.386	1.396	5.658	-10.238	-0.116
DCM	S_0	1.369	1.458	5.673	-0.045	-0.001
(CPCM)	S_1	1.386	1.396	5.658	-10.305	-0.118

C11-N14, one can identify that the bond length decreases as the molecule excites to the S_1 state. This decrease in bond length provides support for the charge transfer characteristic of 3° PABA. Furthermore, when excited from the S_0 to S_1 state, the C4-C3-N14-C15 dihedral angle, which is crucial for TICT emission, changes from -0.044° to -10.238° in BuOH solvent and from -0.045° to -10.305° in DCM solvent. In S_0 geometry, since the -NMe_2 group is planar to the benzene ring; therefore, the lone pair electrons of the nitrogen atom can be delocalized over the benzene ring with relative ease. Furthermore, the twisted geometry at the S_1 state promotes the ICT process in accordance with the TICT model. Next, when 2° PABA is checked with CPCM model, it was observed that the geometrical properties are comparable to those of 3° PABA in both solvents. This implies that 2° PABA is also capable to show both LE and TICT emission. Conversely, if we observe 1° PABA, despite the fact that the C11-N14 bond length decreases, the C4-C3-N14-H15 dihedral angle is not planar to the benzene ring, which diminishes the likelihood of charge transfer as well as dual fluorescence in 1° PABA.

3.2. Potential energy curves

The potential energies at S_0 and S_1 states are calculated as a function of –NR_2 (R = H, Me) twisting angles (C4-C3-N14-R15 dihedral angle, see Fig. 1) for all the molecules in gas phase, BuOH, and DCM using two solvent model systems SMD and CPCM. For calculating the potential energy curves as a function of the said twisting angle, the optimized geometry at S_0 state is taken, and single point energies are calculated for the twisting angle variation from -20 – 120° for 3° and 2° PABA, and from 0° to 180° for 1° PABA at every 10° interval. The same scan for S_1 state is obtained by taking the same geometries of S_0 state at every twisting angle, and energies of S_1 state are calculated using TDDFT methodology. Such a methodology was used in the past several times and claimed to provide an accurate interpretation to the experimental results [44,45].

In Fig. 3, the scan for 3° PABA is shown for gas phase, BuOH, and DCM solvent systems. A clear double well S_1 surface is visible for these figures, one at 0° twisting angle and another at 90°. While the former one is in the FC region and is the one where the LE fluorescence is originated from, the latter at 90° twisting angle is the origin of CT emission spectrum. Thus, the dual emission nature of 3° PABA can be nicely demonstrated from the corresponding potential energy curves of S_0 and S_1 states. It may be important to note that there is a potential barrier for the population to transfer from the former well to the latter. Interestingly, the barrier height reduces significantly in the presence of a more polar solvent, namely, BuOH. For 3° PABA, this potential barrier is 5.87 kcal/mol in gas phase and is 2.15 (2.52) kcal/mol in DCM solvent. In BuOH, the barrier further reduces to 1.78 (0.430) kcal/mol in CPCM (SMD) solvent model. These small barriers are easily accessible even at room temperature (thermal energy, *RT* at 300 K = 0.6 kcal/mol).

In case of 2° PABA, as observed from Fig. 4, there is still enough evidence for dual emission behaviour from the potential energy curves. This has not been experimentally explored yet. However, in terms of the feasibility of the dual emission between 3° and 2° PABA, the potential energy barrier may be compared. The gas phase barrier is 7.46 kcal/mol. In DCM this barrier is 5.30 (5.95 kcal/mol), while in BuOH, the barrier is reduced to 5.17 (3.18) kcal/mol. Therefore, although the potential barrier is not very high for 2° PABA, it is higher than that of 3° PABA, making the latter a better dual emission species. On the other hand, in 1° PABA, there is no evidence of CT emission from the potential energy scan, as depicted in Fig. 5. The potential energy barriers for all molecules

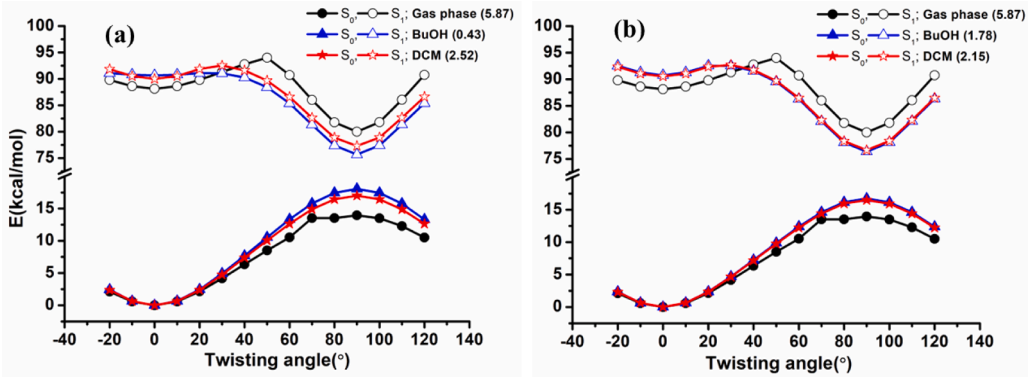

Fig. 3. Potential energy curves for ground and first excited state of 3° PABA with varying the $-NR_2$ twisting angle for gas, BuOH, and DCM with both (a) SMD and (b) CPCM models. The $\Delta E_{LE \rightarrow TICT}$ values (kcal/mol) are written in the parenthesis.

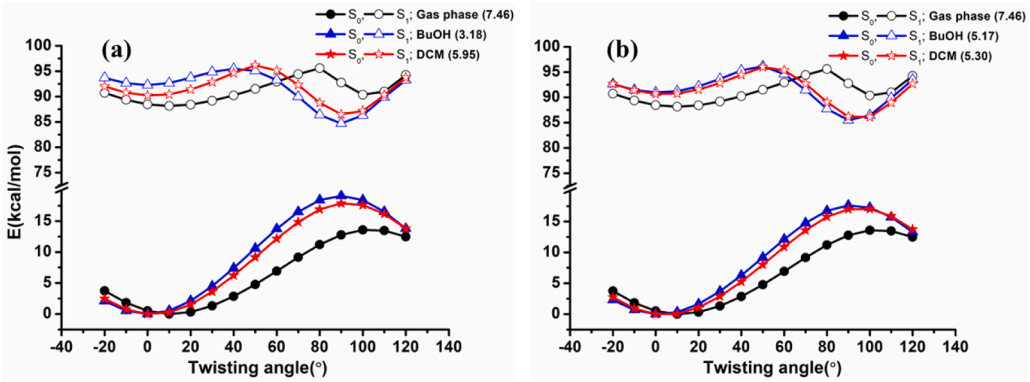

Fig. 4. Same as Fig. 3 but for 2° PABA.

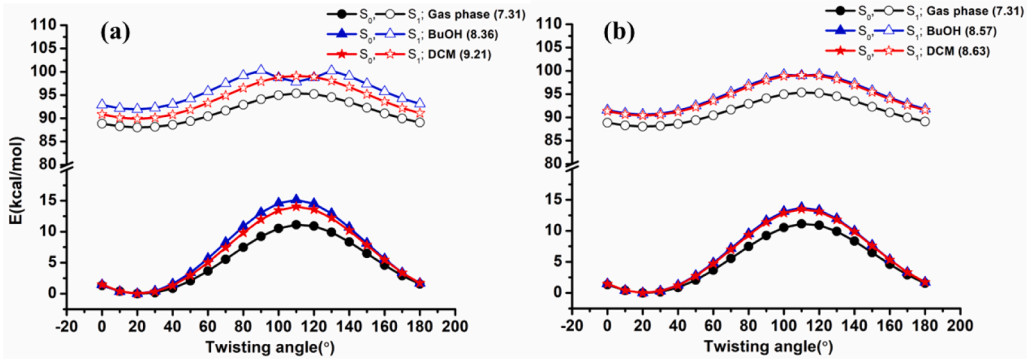

Fig. 5. Same as Fig. 3 but for 1° PABA.

and in all solvent systems are listed in Table 2, which shows an opposite trend. The energy barrier increases from gas phase to BuOH to DCM in both models. The increased potential energy barrier height in 1° PABA could be due to the lack of conjugation of the lone pair of nitrogen in this molecule. As provided in Table S2, the geometry of 1° PABA in S_0 state minimum showed a much higher dihedral angle of NH_2 group with respect to the benzene ring. Hence, the lone pair of nitrogen is not expected to participate in the conjugation as prompt as in 2° or 3° PABA. Thus, in 1° PABA, there will be expectedly only one emission spectra (LE) possible which is to be verified by experiment.

Table 2
Potential energy barrier at S_1 state from LE to TICT emissions.

Medium/Solvent	Solvent Model	Potential Energy Barrier (kcal/mol)		
		3° PABA	2° PABA	1° PABA
Gas Phase	–	5.87	7.46	7.31
BuOH	SMD	0.43	3.18	8.36
	CPCM	1.78	5.17	8.57
DCM	SMD	2.52	5.95	9.21
	CPCM	2.15	5.30	8.63

3.3. Absorption and emission spectra

After understanding the dual emission phenomenon from potential energy scans, the theoretical absorption and emission spectra are computed for all these molecules. For 3° PABA the spectra are compared with the experiment. The absorption spectra of all the molecules are for the $\pi \rightarrow \pi^*$ transition and are presented in Fig. 6 for gas phase

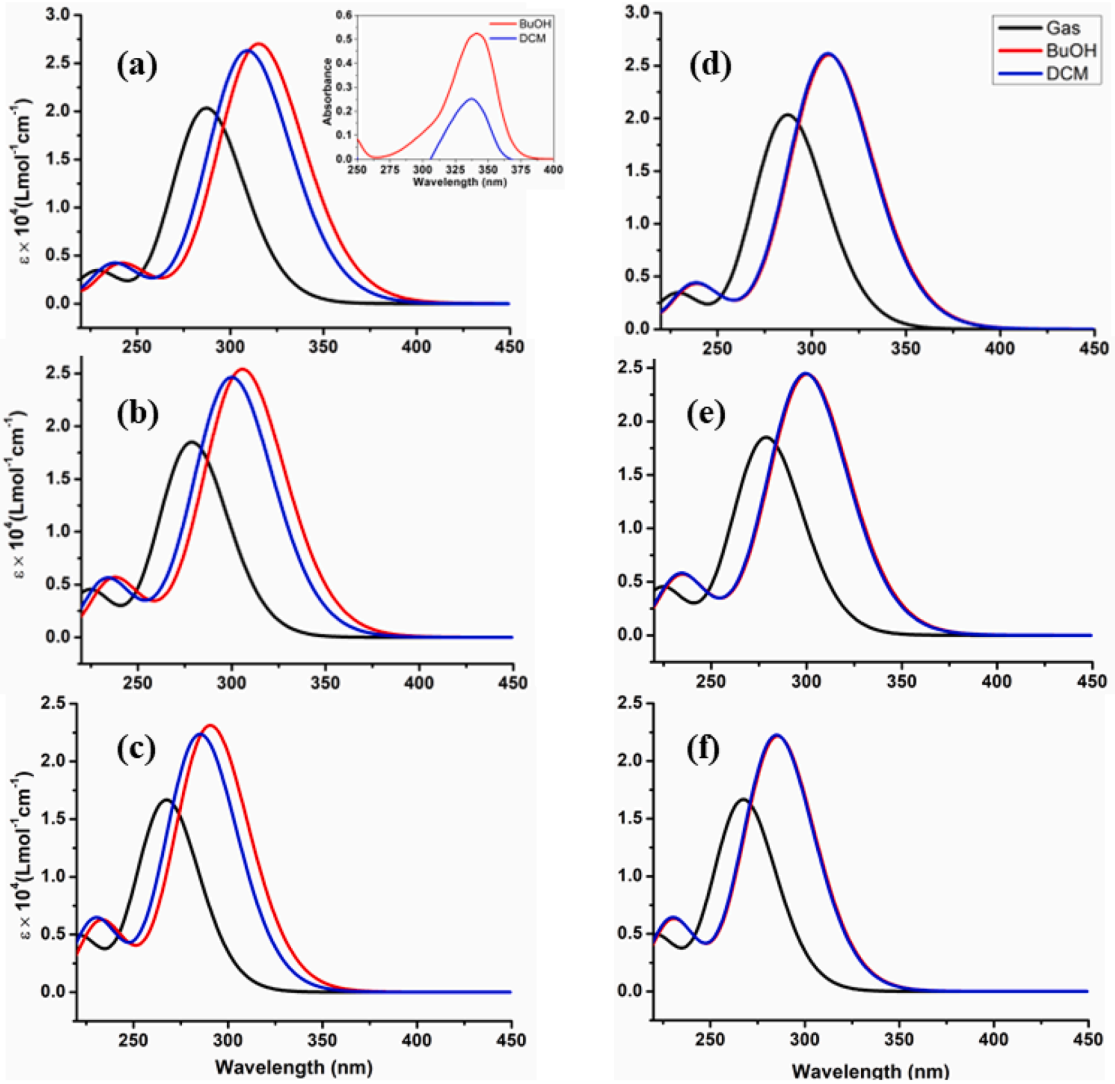

Fig. 6. Absorption spectra for 3° PABA (a) and (d), 2° PABA, (b) and (e), and 1° PABA, (c) and (f) in gas, BuOH, and DCM solvent with SMD, (a), (b), and (c), and CPCM (d), (e), and (f) models. Experimental absorption spectrum of 3°PABA is shown in the inset of (a) for both BuOH and DCM solvents.

Table 3
The computed absorption and local emission (LE) λ_{max} and the corresponding energy gaps (ΔE).

Molecule	Solvent	Model	Absorption λ_{max}(nm)	ΔE (kcal/mol)	Emission λ_{max}(nm)	ΔE (kcal/mol)
3° PABA	Gas Phase	–	287.7	99.37	297.3	96.18
	BuOH	SMD	315.4	90.65	327.5	87.31
	DCM		309.5	92.38	321.8	88.86
	BuOH	CPCM	309.5	92.39	321.9	88.81
	DCM		308.8	92.59	321.3	89.00
2° PABA	Gas Phase	–	279.7	102.2	288.4	99.15
	BuOH	SMD	306.0	93.44	319.5	89.50
	DCM		300.6	95.13	310.4	92.11
	BuOH	CPCM	300.6	95.12	310.6	92.04
	DCM		299.5	95.36	310.0	92.22
1° PABA	Gas Phase	–	268.0	106.7	276.6	103.4
	BuOH	SMD	290.8	98.32	300.0	95.30
	DCM		285.5	100.1	295.3	96.82
	BuOH	CPCM	285.8	100.0	295.4	96.79
	DCM		285.3	100.2	295.1	96.89

calculations and in BuOH and DCM solvents using both CPCM and SMD models. In Table 3, the λ_{max} values for both the absorption and local emission (LE) spectrum are reported along with the corresponding energy gaps.

The absorption curves show a blue shift for the λ_{max} moving from 3° PABA to 2° to 1° The λ_{max} in gas phase for tertiary, secondary, and primary PABA are 288, 280, and 268 nm. This suggests that the energy gap between S_0 and S_1 states increases from 3° PABA to 1° PABA. The corresponding energy gaps are 99.37, 102.2, and 106.7 kcal/mol in gas phase. This may be due the destabilization of the excited state by weakening the electron donation ability of amine group from 3° to 1° PABA. This situation is also consistent in the calculations in presence of solvents. For SMD model, the energy gaps are 90.65 for tertiary, 93.44 for secondary, and 98.32 kcal/mol for primary PABA in BuOH. On the other hand, for a particular molecule, there is a redshift from gas phase to solvent phase. For example, the λ_{max} values for 3° PABA are 288, 309, and 315 nm in gas phase, DCM and BuOH, respectively in SMD model. In the same model, the peak in BuOH shows a significant redshift than the one in DCM solvent. In CPCM model, the redshift is not so significant. The charge separation in the excited state gets stabilized in polar solvent. As a result, there is a redshift form gas phase absorption to solvent phase. BuOH, being more polar than DCM, the absorption maxima shift towards higher wavelength further. For SMD model, the energy gap in

DCM is ~1.7 kcal/mol higher than that in BuOH for the 3° PABA. This difference of energy gaps for 2° and 1° PABA are also very similar and are ~1.7 and ~1.8, respectively (see Table 3).

In Fig. 7, the LE spectra are shown for all molecules as calculated from gas and solvent phases using both SMD and CPCM models. The emission spectra are also similar to the absorption spectra mentioned above. The λ_{max} values are 297, 328, and 322 nm for tertiary PABA in gas phase, BuOH, and DCM, respectively, in SMD model. These values for 2° PABA are 288, 319, and 310 nm, and for 1° PABA are 277, 300, and 295 nm. As one can see, there is a consistent blue shift from 3° PABA to 1° PABA. On the contrary, for a particular molecule, there is a red shift from gas phase to DCM to BuOH. This observation of LE is similar to the absorption phenomenon. However, for 3° PABA and in gas phase, the energy gap from absorption data was obtained as 99.37 kcal/mol. From LE spectra, this gap is reduced to 96.18 kcal/mol. In case of BuOH and DCM, this lowering of energy values are 3.34, and 3.52 kcal/mol, respectively for 3° PABA in SMD model (see Table 3). In the cases of 2° and 1° PABA, this energy gap difference is ranging from 3 – 4 kcal/mol. Such a gap is expected mainly due to vibrational relaxation after the absorption and before the emission.

For the TICT emission spectra, the theoretical oscillator strength was calculated to be zero or very small, hence the pictorial representation could not be presented. This may be due the forbidden transition in the theoretical procedure [46]. Experimentally, the TICT spectrum can be obtained due to the vibronic coupling [46]. In this calculation, the molecules are first optimized at S_1 state with 90° –NR_2 twisting angle (C4-C3-N14-R15 dihedral angle, see Fig. 1) with respect to the benzene ring. Then, this optimized geometry is considered at S_0 state, and an absorption spectrum is calculated with TDDFT method. This absorption spectrum is nothing but the TICT emission spectrum. In Table 4, the

Table 4
The wavelengths with the corresponding oscillator strengths for the TICT emission spectra of 3°, 2°, and 1° PABA molecules.

Medium/ Solvent	Solvent Model	Wavelength (Oscillator Strength)		
		3° PABA	2° PABA	1° PABA
Gas Phase	–	514.30 (0.0000)	419.46 (0.0014)	–
BuOH	SMD	595.16 (0.0001)	493.28 (0.0000)	376.04 (0.0001)
	CPCM	572.47 (0.0000)	477.70 (0.0000)	390.76 (0.0000)
DCM	SMD	561.16 (0.0002)	468.30 (0.0015)	–
	CPCM	567.07 (0.0000)	471.98 (0.0013)	–

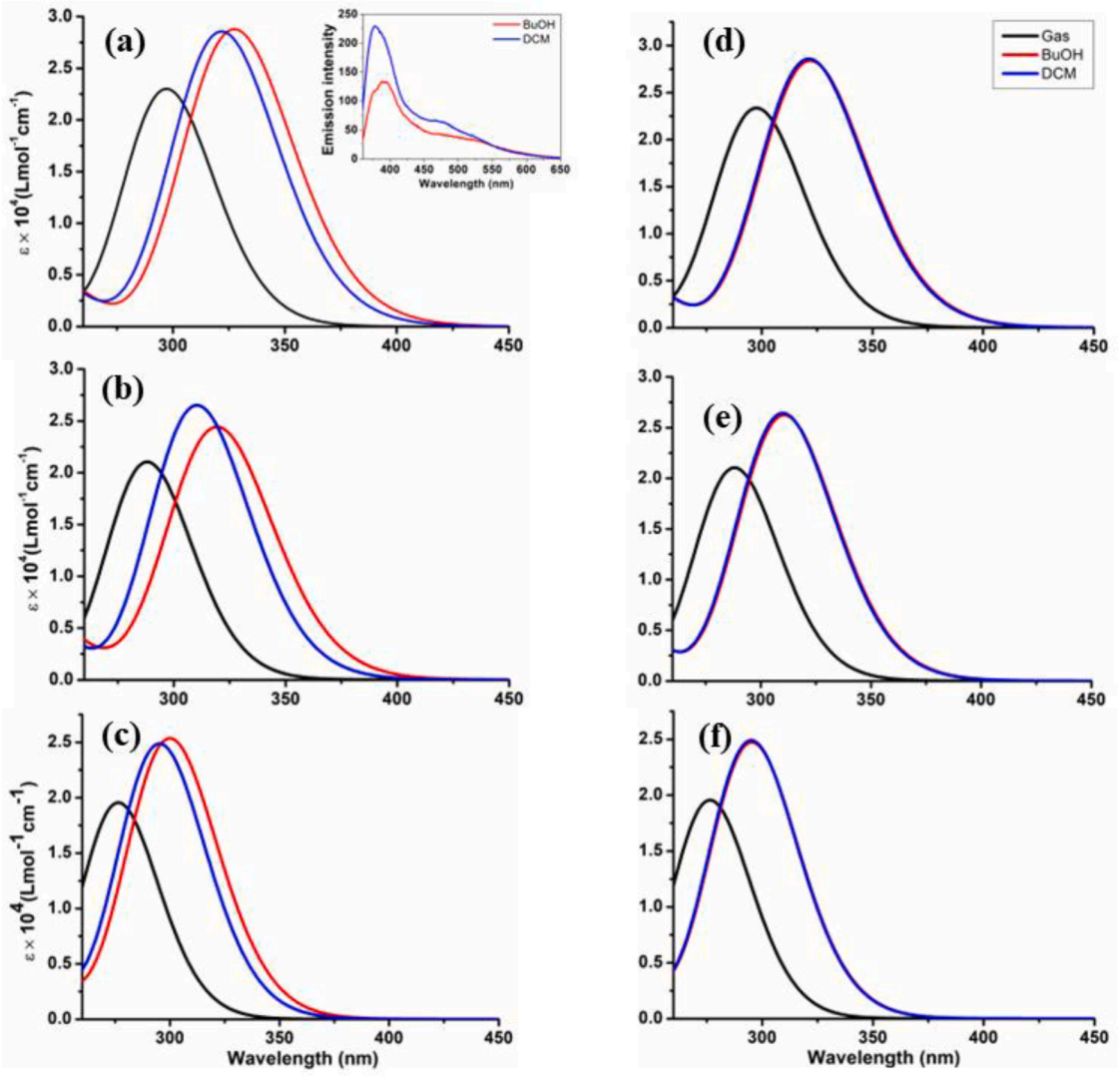

Fig. 7. Local Emission (LE) spectra for 3° PABA (a) and (d), 2° PABA, (b) and (e), and 1° PABA, (c) and (f) in gas, BuOH, and DCM solvent with SMD, (a), (b), and (c), and CPCM (d), (e), and (f) models. Experimental LE spectrum of 3°PABA is shown in the inset of (a) for both BuOH and DCM solvents.

wavelengths of the TICT emission spectrum of all the molecules are presented.

As one can see from Table 4, the TICT emissions are taking place at wavelengths above 500 nm and ranging from 514 to 595 nm. Experimental observations are also similar but somewhat lower than the theoretical ones. For 3° PABA, the experimental λ_{max} are 492 and 505 nm in DCM and BuOH solvents [8]. The theoretical values are 561 nm (SMD) and 567 nm (CPCM) in DCM, and 595 nm (SMD) and 572 nm (CPCM) in BuOH. The mismatch may be due to the theoretical methods employed for the current work. However, in the earlier works [18,19], the TICT emission was reported at ~600 nm in DMF and ACN solvents, which are not considered in the present work.

Another observation in the present calculations is that there is a minimum in S_1 state at 90° twisting angle for 1° PABA in BuOH solvent for both SMD and CPCM models, as seen in Fig. 5b. Such minimum was absent in gas phase and DCM calculations. Therefore, an emission spectrum was also obtained for this molecule at that geometry. However, the associated wavelength is at the lower side, as reported in Table 4. For the gas phase and DCM solvent there is no minimum located at 90° twisting angle (see Fig. 5a and c) and hence, no TICT emission spectrum was obtained.

3.4. Excited state dynamics

To check the possibility of the molecules to produce TICT emission spectrum, the dynamics at the S_1 state is performed in the gas phase based on the procedure mentioned in Section 2 for all the 3°, 2°, and 1° PABA. The starting geometry of this molecule is around the S_0 optimized geometry, i.e., at the twisting angle around 0°. Due to a probability window of 0.5 eV, the initial twisting angle varied around -30° to 30°, but much lesser than 90°. In Fig. 8 (a), (b), (c), the change in twisting angle is measured as the dihedral angle of C4-C3-N14-R15 (see Fig. 1) as a function of simulation time for all PABA molecules. As one can see that in case of 3° PABA, many trajectories show a final twisting angle around 90°. From the data, about 36 % of trajectories ended with a twisting angle (absolute value) range of 60–120° at 300 fs. There is no trajectory found in this molecule, which ended at around 180°. In case of 2° PABA, some trajectories ended with a twisting angle of 180° (~4 %), which means the molecule returns back to a structure similar to the original one with an interchange of the position of H and CH_3 of the amine group.

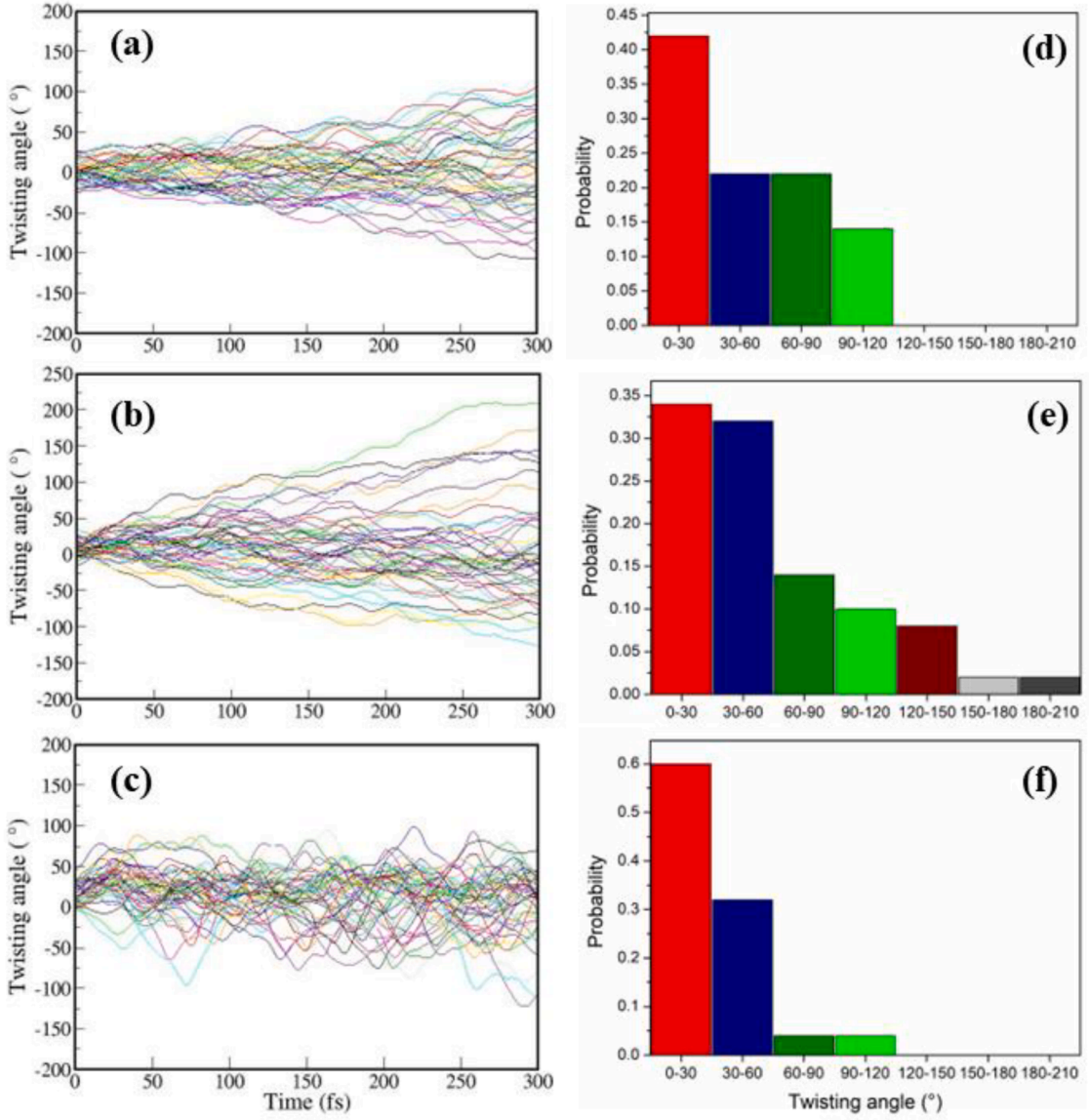

Fig. 8. Twisting angle as a function of simulation time for 3° (a), 2° (b), and 1° (c) PABA and probability distribution of the twisting angle at the end of the simulation for 3° (d), 2° (e), and 1° (f) PABA.

Moreover, 24 % of the trajectories for 2° PABA remained with a twisting angle (absolute value) range of 60 - 120° at 300 fs. Interestingly, for 1° PABA, the angle varies randomly between ±90°. One can understand the behaviour by looking at the potential energy curves shown in Figs. 3, 4, and 5. The TICT (at twisting angle of 90°) potential energy well is deeper in 3° PABA, shallower in 2° PABA, and no potential energy well at all in 1° PABA in the gas phase. As a result, the molecule is better trapped when tertiary molecule is considered than for the secondary.

The bar diagram at 300 fs, as shown in Fig. 8 (d), (e), and (f) demonstrates that for 3° PABA, a greater number of trajectories are seen to stick to ~90° twisting angle towards the end of the simulation in case of 3° PABA and no trajectories are found with twisting angle 120° or more. In case of 2° PABA, although a significant number of molecules are produced with 90° twisting angle, some of them (about 12 %) are found to form the end products with a twisting angle range of 120–210°. This is because of a shallower potential well in 2° PABA than in case of 3° PABA. With no potential well, 1° PABA, shows a smaller number of molecules with a twisting angle of 90° at the end of trajectories integration. There are 8 % of the trajectories ended with a twisting angle range of 70–110°, and no trajectories are found to end with a twisting angle of 180°. It may be noted that all the dynamical calculations are performed at 0 K temperature. The energy acquired by the molecules to cross the S_1 potential barrier from LE minimum to TICT minimum could be due to the zero-point energy leakage in the classical dynamics. If the temperature was more, the percentages of the twisted molecule could have been more, but the overall comparative scenario may not be altered.

4. Summary

The current article contributes to the understanding of dual emission property in the light of twisted intramolecular charge transfer (TICT) phenomenon and helps to construct the model which may show such property. This theoretical work demonstrates the dual emission properties of primary (1°), secondary (2°), and tertiary (3°) *p*-aminobenzaldehyde (PABA) and exhibits the possibilities of TICT. The study was performed in gas phase, in butanol (BuOH), and in dichloromethane (DCM) solvents. The potential energy scan with respect to the twisting angle of amine group of the molecules showed that 3° and 2° PABA are the potential candidates for the dual emission behaviour, whereas 1° PABA could only exhibit local emission. Excited state molecular dynamics simulations, as performed in the gas phase also suggest that 3° PABA has a longer lifetime at the 90° twisting angle of the amine group, making it a more efficient dual emitter. For 2° PABA, although the molecules are produced with 90° twisting angle with similar probability of 3° PABA, the lifetime is shorter. 1° PABA, on the other hand, did not show any considerable lifetime at 90° twisting angle geometry.

This work presents the possibilities of excited state charge transfer for a weak donor-acceptor model. This study could pave the way of modelling molecular structures for dual emission property and can be used to understand excited state charge transfer, excited state proton transfer behaviours, etc. It also suggests the future directives of the experimental investigations in this field.

CRediT authorship contribution statement

Palash Jyoti Boruah: Investigation, Formal analysis, Data curation. **Venkatesh N:** Visualization, Investigation. **Anuva Samanta:** Investigation, Conceptualization. **Amit Kumar Paul:** Writing – review & editing, Writing – original draft, Supervision, Funding acquisition.

Declaration of competing interest

The authors declare that they have no known competing financial interests or personal relationships that could have appeared to influence the work reported in this paper.

Data availability

Data will be made available on request.

Acknowledgment

AKP would like to acknowledge SERB funding with file no. CRG/2022/003033, AKP, and AS would like to acknowledge Nikhil Guchhait for fruitful academic discussion related to this work, PJB would like to acknowledge NIT Meghalaya and MoE for his fellowship. VN likes to acknowledge NIT Meghalaya for providing the research facilities.

Supplementary materials

Supplementary material associated with this article can be found, in the online version, at doi:10.1016/j.chphi.2024.100538.

References

[1] E.M. Kosower, H. Dodiuk, Multiple fluorescences. II. A new scheme for 4-(N,N-dimethylamino)benzonitrile including proton transfer, J. Am. Chem. Soc. 98 (1976) 924.
[2] E. Lippert, W. Lüder, F. Moll, H. Nagele, H. Boos, H. Prigge, I. Siebold-Blankenstein, Umwandlung von elektronenanregungsenergie, Angew. Chem. 73 (1961) 695.
[3] Z. Grabowski, J. Dobkowski, Twisted intramolecular charge transfer (TICT) excited states: energy and molecular structure, Pure Appl. Chem. 55 (1983) 245.
[4] A.L. Sobolewski, W. Sudholt, W. Domcke, Ab initio investigation of reaction pathways for intramolecular charge transfer in dimethylanilino derivatives, J. Phys. Chem. A 102 (1998) 2716.
[5] W. Rettig, Charge separation in excited states of decoupled systems—TICT compounds and implications regarding the development of new laser dyes and the primary process of vision and photosynthesis, Angew. Chem. Int. Ed. Engl. 25 (1986) 971.
[6] A. Gorse, M. Pesquer, Intramolecular charge transfer excited state relaxation processes in para-substituted N,N-dimethylaniline: a theoretical study including solvent effects, J. Phys. Chem. 99 (1995) 4039.
[7] D. Rappoport, F. Furche, Photoinduced intramolecular charge transfer in 4-(Dimethyl) aminobenzonitrile – a theoretical perspective, J. Am. Chem. Soc. 126 (2004) 1277.
[8] A. Samanta, B.K. Paul, N. Guchhait, Reinvestigation of photoinduced intramolecular charge transfer reaction in p-Dimethylaminobenzaldehyde by spectroscopic method and density functional theory (DFT) calculation, J. Lumin. 132 (2012) 517.
[9] J.J. La Clair, An atmospherically driven optical switch, Angew. Chem. Int. Ed. Engl. 38 (1999) 3045.
[10] J.P. Lakowicz, Principles of Fluorescence Spectroscopy, 2nd ed., Kluwer Academic/Plenum Press, New York, 1999.
[11] B. Kippelen, H.S. Lackritz, R.O. Claus, Organic Nonlinear Optical Material and Devices, Materials Research Society, P. A., 1999.
[12] B. Lama, M. Sarma, Unraveling the mechanistic pathway for the dual fluorescence in green fluorescent protein (GFP) chromophore analogue: a detailed theoretical investigation, J. Phys. Chem. B 126 (2022) 9930.
[13] K. Rotkiewicz, K.H. Grellmann, Z.R. Grabowski, Reinterpretation of the anomalous fluorescense of p-N,N-dimethylamino-benzonitrile, Chem. Phys. Lett. 19 (1973) 315.
[14] Z.R. Grabowski, J. Dobkowski, W. Kuhnle, Model compounds in study of the photophysical behaviour of carbonyl derivatives of N, N-dimethylaniline, J. Mol. Struct. 114 (1984) 93.
[15] W. Schuddeboom, S.A. Jonker, J.M. Warman, U. Leinhos, W. Kuhnle, K. A. Zachariasse, Excited-state dipole moments of dual fluorescent 4-(dialkylamino) benzonitriles: influence of alkyl chain length and effective solvent polarity, J. Phys. Chem. 96 (1992) 10809.
[16] K.A. Zachariasse, M. Grobys, Th. Haar, A. Hebecker, Yu.V. Il'ichev, Y.B. Ziang, O. Morawski, W. Kuhnle, Intramolecular charge transfer in the excited state. Kinetics and configurational changes, J. Photochem. Photobiol. A Chem. 102 (1996) 59.
[17] K.A. Zachariasse, M. Grobys, Th. Haar, A. Hebecker, Yu.V. Il'ichev, O. Morawski, I. Ruckert, W. Kuhnle, Photo-induced intramolecular charge transfer and internal conversion in molecules with a small energy gap between S_1 and S_2. Dynamics and structure, J. Photochem. Photobiol. A Chem. 105 (1997) 373.
[18] A. Kawski, B. Kukliński, P. Bojarski, Excited state dipole moments of 4-(dimethylamino)benzaldehyde, Chem. Phys. Lett. 448 (2007) 208.
[19] Z. Grabowski, K. Rotkiewicz, W. Rettig, Structural changes accompanying intramolecular electron transfer: focus on twisted intramolecular charge-transfer states and structures, Chem. Rev. 103 (2003) 3899.
[20] S. Kundu, N. Chattopadhyay, Dual luminescence of dimethylaminobenzaldehyde in aqueous β-cyclodextrin: non-polar and TICT emissions, J. Photochem. Photobiol. A Chem. 88 (1995) 105.

[21] S. Kundu, N. Chattopadhyay, Twisted intramolecular charge transfer of dimethylaminobenzaldehyde in α-cyclodextrin cavity, J. Mol. Struct. 344 (1995) 151.
[22] R.M. Krieger, P.W. Jagodzinski, Catalytic oxidation of 4-(dimethylamino) benzaldehyde by gold nanoparticles. Part I: Reaction characterization, J. Mol. Struct. 876 (2008) 56.
[23] J. Choi, K. Yeo, M. Yoon, S.J. Lee, K. Kim, Photoinduced intramolecular charge-transfer state of p-dimethylaminobenzoic acid in CdS and TiO2 colloid solutions, J. Photochem. Photobiol. A Chem. 132 (2000) 105.
[24] Y. Yang, Y. Zhao, W. Shi, F. Ma, Y. Li, Colorimetric fluorescence probe detecting Hg2+ and OCl– based on intramolecular charge transfer and excited-state intramolecular proton transfer mechanisms, J. Lumin. 209 (2019) 102.
[25] L. Yang, D. Zhang, M. Wang, Y. Yang, Effects of solvent polarity on the novel excited-state intramolecular thiol proton transfer and photophysical property compared with the oxygen proton transfer, Spectrochim. Acta Part A Mol. Biomol. Spectrosc. 293 (2023) 122475.
[26] M.A. Kochman, B. Durbeej, Simulating the nonadiabatic relaxation dynamics of 4-(N,N-Dimethylamino)benzonitrile (DMABN) in polar solution, J. Phys. Chem. A 124 (2020) 2193–2206.
[27] K. Issler, F. Sturm J. Petersen, M. Flock, R. Mitrić, I. Fischer, L. Barreau, L. Poisson, Time-resolved photoelectron spectroscopy of 4-(dimethylamino)benzethyne – an experimental and computational study, Phys. Chem. Chem. Phys. 25 (2023) 9837.
[28] Y. Zhang, C. Shang, Y. Cao, C. Sun, Quantum mechanics/molecular mechanics studies on the photoprotection mechanisms of three chalcones, J. Mol. Liq. 372 (2023) 121165.
[29] C. Shang, C. Sun, Substituent effects on photophysical properties of ESIPT-based fluorophores bearing the 4-diethylaminosalicylaldehyde core, J. Mol. Liq. 367 (2022) 120477.
[30] Y. Li, B. Cao, Q. Zhou, X. Zhang, B. Li, X. Su, Y. Shi, Enhancing fluorescence of benzimidazole derivative via solvent-regulated ESIPT and TICT procesS: A TDDFT study, Spectrochim. Acta Part A Mol. Biomol. Spectrosc. 258 (2021) 119862.
[31] Y. Wan, B. Li, Y. Liu, D. Wang, L. Zhu, Q. Li, H. Yin, C. Liu, M. Jin, J. Gao, Y. Shi, Turn-on stimuli-responsive switch: strategies for activating a new fluorescence channel by pressure, Opt. Express 31 (2023) 13017–13027.
[32] A.D. Becke, Density-functional thermochemistry. III. The role of exact exchange, J. Chem. Phys. 98 (1993) 5648.
[33] C. Lee, W. Yang, R.G. Parr, Development of the Colle-Salvetti correlation-energy formula into a functional of the electron density, Phys. Rev. B 37 (1988) 785.
[34] R. Ditchfield, W.J. Hehre, J.A. Pople, Self-consistent molecular-orbital methods. IX. An extended gaussian-type basis for molecular-orbital studies of organic molecules, J. Chem. Phys. 54 (2003) 724–728.
[35] W.J. Hehre, R. Ditchfield, J.A. Pople, Self—consistent molecular orbital methods. XII. Further extensions of Gaussian—type basis sets for use in molecular orbital studies of organic molecules, J. Chem. Phys. 56 (2003) 2257.
[36] M.J. Frisch, J.A. Pople, J.S. Binkley, Self-consistent molecular orbital methods 25. Supplementary functions for Gaussian basis sets, J. Chem. Phys. 80 (1984) 3265.
[37] M. Cossi, N. Rega, G. Scalmani, V. Barone, nergies, structures, and electronic properties of molecules in solution with the C-PCM solvation model, J. Comput. Chem. 24 (2003) 669–681.
[38] A.V Marenich, C.J. Cramer, D.G. Truhlar, Universal solvation model based on solute electron density and on a continuum model of the solvent defined by the bulk dielectric constant and atomic surface tensions, J. Phys. Chem. B 113 (2009) 6378.
[39] M.J. Frisch; G.W. Trucks; H.B. Schlegel; G.E. Scuseria; M.A. Robb; J.R. Cheeseman; G. Scalmani; V. Barone; B. Mennucci; G.A. Petersson, et al. Gaussian 09, Revision E.01, Wallingford CT, 2009.
[40] MM. Barbatti, M. Ruckenbauer, F. Plasser, J. Pittner, G. Granucci, M. Persico, H. Lischka, Newton-X: a surface-hopping program for nonadiabatic molecular dynamics, WIREs Comput. Mol. Sci. 4 (2014) 26.
[41] H. Lischka, T. Müller, P.G. Szalay, I. Shavitt, R.M. Pitzer, R. Shepard, Columbus—a program system for advanced multireference theory calculations, WIREs Comput. Mol. Sci. 1 (2011) 191.
[42] B.O. Roos, P.R. Taylor, P.E.M. Sigbahn, A complete active space SCF method (CASSCF) using a density matrix formulated super-CI approach, Chem. Phys. 48 (1980) 157.
[43] B.O. Roos, P. Linse, P.E.M. Siegbahn, M.R.A. Blomberg, A simple method for the evaluation of the second-order-perturbation energy from external double-excitations with a CASSCF reference wavefunction, Chem. Phys. 66 (1982) 197.
[44] J.M. Ortiz-Sánchez, R. Gelabert, M. Moreno, J.M. Lluch, Theoretical study on the excited-state intramolecular proton transfer in the aromatic schiff base salicylidene methylamine: an electronic structure and quantum dynamical approach, J. Phys. Chem. A 110 (2006) 4649.
[45] S. Mahanta, R.B. Singh, S. Kar, N. Guchhait, Evidence of coupled photoinduced proton transfer and intramolecular charge transfer reaction in para-N,N-dimethylamino orthohydroxy benzaldehyde: Spectroscopic and theoretical studies, Chem. Phys. 354 (2008) 118.
[46] J.B. Foresman, Æ. Frisch, Exploring Chemistry with Electronic Structure Methods, 3rd ed., Gaussian, Inc., Wallingford, CT, 2015, p. 333.